JP&M Engineering
Journal of Petroleum and Mining Engineering
http://jpme.journals.ekb.eg/

Failure analysis of heat exchanger tubes of Ni-200 alloy in a titanium tetrachloride vaporizer

Ashraf Bakkar [a,b,*], Sabbah Ataya [a,d], Ossama Badr [c]

[a] Metallurgical and Materials Engineering Department, Faculty of Petroleum and Mining Engineering, Suez University, 43721 Suez, Egypt.
[b] Department of Environmental Engineering, College of Engineering at Al-Lith, Umm Al-Qura University, Saudi Arabia.
[c] Cristal Global, Saudi Arabia
[d] College of Engineering, Al Imam Mohammad Ibn Saud Islamic University (AMSIU), 11432 Riyadh, Saudi Arabia.

*Corresponding author e-mail: ashrafbakkar@yahoo.com

Article Info

Received 19 Jan. 2020
Revised 7 Feb. 2020
Accepted 12 Feb. 2020

Keywords

Failure analysis; Corrosion; Heat exchanger, Nickel; Titanium tetrachloride

Abstract

This paper presents a metallurgical analysis of damage occurred in heat exchanger tubes of nickel alloy (Ni-200) used for vaporizing titanium tetrachloride ($TiCl_4$). The tubes had undergone a dual environmental condition with heating water steam inside and liquidous $TiCl_4$ outside. Several investigations were conducted to identify the potential failure mechanism. Such investigations included visual examination and microstructural characterization via optical microscopy and scanning electron microscopy (SEM) equipped with energy dispersive X-ray analyzer (EDX). Investigations extended also to the mechanical characterization of the tube materials through hardness and tensile testing. The results of hardness and tensile tests showed that the bent tubes had sustained strain hardening, which can act as potential sites of corrosion. SEM and EDX investigations revealed that the damaged sections had corrosion product layers rich in sulfur. However, cavitation corrosion was found to be the main corrosion form shown in the damaged tubes. It is recommended to keep $TiCl_4$ liquid at high pressure values so that the vapor bubbles are not formed. Also, the sulfur content in the $TiCl_4$ must be kept at very low levels.

Introduction

Nickel is well known as one of the most important metals and has wide applications due to its good mechanical properties and its high corrosion resistance in aggressive atmospheres and most of corrosive media. Its high corrosion resistance is due to formation of a protective passive film in neutral, near neutral and alkaline media. Nickel is highly resistant to corrosion by steam as a result of formation of protective passive film on its surface [1,2,3]. However, its corrosion resistance decreases in steam containing carbon dioxide and air [4]. Nickel has ultra corrosion resistance to titanium chloride melts. It has been reported that Ni has superior corrosion resistance for titanium chlorides over titanium, molybdenum, stainless steel alloys, and higher-chromium super alloys [5,6].

Various degradation mechanisms are characterized in heat exchangers due to interaction between the metal, the environment (inside and outside the tubes), and the mechanical conditions [7,8,9]. The failure of a heat exchanger raises questions about the cause of failure, which one or more of four main causes; corrosion, mechanical, mechanical induced corrosion, or scale- mud- and algae-fouling [10]. The corrosion of heat exchangers has been reported to be in general corrosion form or many localized corrosion forms such as galvanic corrosion, pitting, intergranular corrosion, crevice corrosion, microbiologically influenced corrosion (MIC), erosion corrosion, stress corrosion cracking (SCC), hydrogen embrittlement, etc [11].

Operating conditions

The applied Ni-200 alloy tubes are annealed at 800°C after production and bended at Cristal Yanbu site by cold bending process to U-form. The manufactured tube bundle is utilized in titanium tetrachloride ($TiCl_4$) vaporizer without heat treatment after bending. The typical chemical composition of the Ni-200 tubes is listed in Table 1 compared with the nominal composition according to ASTM B13.

The tube bundle is immersed in a fluid of $TiCl_4$, containing $AlCl_3 \leq 1.5$ wt.%, $SnCl_4 \leq 0.7$ wt.%, and

sulfur with contents range between 40 ppm and 90 ppm. Fig. 1 represents the tube bundle vaporizer in which the liquid $TiCl_4$ enters from the inlet nozzle in the bottom at 128 ^oC and leaves as vapor at 166 ^oC from the outlet nozzle at the top of vaporizer. Inside the Ni-200 alloy tubes, steam is flowing at a temperature of 202 ^oC and a pressure of 15 barg (absolute pressure as per gauge reading) with flow rate of 1050 kg/hr.

Field observations

It has been found that the tubes were undergoing damage in forms of severe pattern of pitting, leakage, and fracture. The tubes that encountered damage were in the top rows at the bending region in the upper left side in the vaporizer, see Fig. 1. The damage mode and fracture due to thinning after attack of the tubes at the bending region are shown in Fig. 2.

h1: optimum liquid level P1: pressure at h1

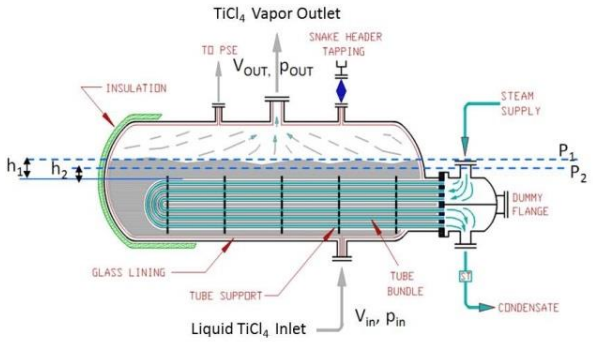

h2: reduction in liquid level P2: pressure at h2

Fig. 1: schematic drawing of titanium tetrachloride vaporizer

Experimental work

Inspection methods were conducted on Ni-200 alloy tubes, as received and after failure, including visual observation, hardness measurements, elemental analysis, and microstructural investigations by optical microscopy (OM) and scanning electron microscopy (SEM) equipped with EDX.

Tensile and hardness tests were conducted on some samples after service, as well as, on the new Ni-200 tubes.

Table 1: Typical chemical composition of the Ni-200 alloy compared with the nominal composition.

Element (wt. %)	Ni	Cu	Fe	Mn	C	Si	S
Typical	99.01	0.14	0.21	0.22	0.13	0.30	0.01
Nominal (ASTM B13)	99 min	0.25 max	0.40 max	0.35 max	0.15 max	0.35 max	0.01 max

(a) (b)

Fig. 2: Damage mode (a) and fracture after thinning (b) on the tubes at the bending region.

tensile test was conducted on test samples taken from the straight part of the used U-formed tube (Fig. 3), using the Universal testing machine Type Instron 4210 (300 kN). The full tube (ϕ=19 $\pm$05 mm and wall thickness T = 2.77 mm) was used for tensile testing. A whole sample length of at least 150 mm was used, where at least 50 mm has been inserted in each grip and the test length was 50 mm according to ASTM A370. The machine speed was 0.015 mm/s which corresponds to the quasi-static strain rate (~ 0.001 s^{-1}). To avoid slipping or folding of the tube on gripping by the tensile testing machine, a steel rod with a diameter just smaller than the internal diameter of the tube was inserted in the tube with a length equal to the gripping length to avoid crushing of the tube, as recommended by ASTM A370 . Three samples of each the old and the new tube materials were tested.

Samples for hardness test were taken from three regions in the U-formed tube as shown in Fig. 3; at the start of curvature (0°), at the mid-way of the curve (45°), and at the nose (90°) of the U-formed tube. The hardness tests were conducted using a low-load Vickers hardness tester with a load of 300 g and dwell time of 30 s.

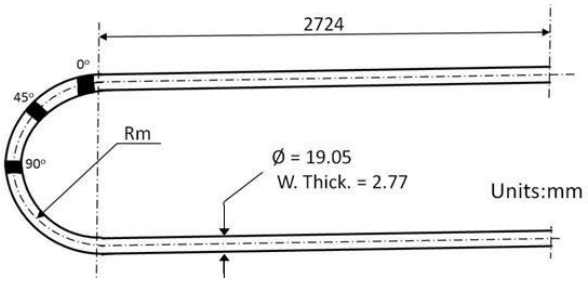

Fig. 3: U-form bent tube showing some dimensions and the location of the taken samples for hardness test (at 0°, 45°, and 90°).

The microstructure was investigated using the Quanta FEG 250 scanning electron microscopy (SEM) equipped with EDX and EBSD systems. EDX analysis for elemental and phase maps was carried out using a scan step size of 0.3 µm.

Results and Discussion

Visual Inspection

Damaged parts were cut from heat exchanger. Fig. 4 shows deteriorated part of the tube at the bended region. The surface suffered from attack resulting in rough topography, while the outer bent fibers showed severe thinning leading to repeated holes as shown in Fig. 4b. The holes are elongated with the length of the tube coinciding with the thinned outer fiber of the bent tube.

Tensile and hardness results

Tensile stress-strain curves of the new samples and the after-service tube samples are shown in Fig. 5. The service life of the old tube samples is around 6 months. The after-service tensile samples showed a clear scattering in the stress-strain curves due to differences in the damage occurred in the tubes, while the new samples revealed a considerable resemblance in the tensile stress-strain curves obtained. Table 2 shows the average tensile test results of the new and the after-service samples. However, the after-service properties showed a clear decrease of the properties due to the damage occurred after the service life.

Hardness testing was applied on the bent tubes to show the effect of bending on the bent region, which may cause strain hardening and consequently residual stresses compared with the un-formed tube.

Fig. 6 shows the results of Vickers's hardness testing on new and old tubes as well as at different positions of the bent tubes. The results showed a notable decrease in the hardness of old tube compared to the new one. For the formed tubes, it is clear that decreasing the bend radius has led to higher hardness values that can be accompanied with higher residual stresses. The top part of the hardness columns in Fig. 6 represents the standard deviation, which was high in the samples from the regions (0°) and (90°). At these regions the scattering of the hardness results was significant due to the differences in strain hardening on the outer wall of the tube (tensile side) at differentially deformed positions over the curved part of the tubes. The residual stresses are tensile on the outer tube wall fibers of bending curvature and compressive on fibers of the inner curvature.

The broadly increasing in the hardness values with the decrease in bend radius indicates that the tube material "Ni-200 alloy" is very strain hardening sensitive, as shown from the tensile stress-strain curves, Fig. 5; The alloy started to yield at about 135 MPa and hardened with the strain to reach nearly four times of the yield stress at the ultimate tensile stress of 511 MPa. Because of the absence of subsequent annealing to the forming process, differential material stability due to the different hardening conditions can represent a potential site for corrosion.

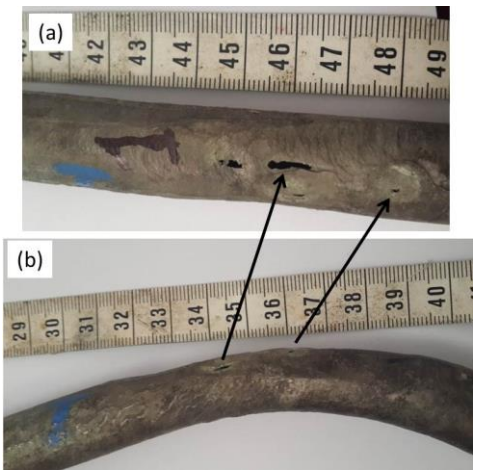

Fig. 4: (**a**) holes in the damaged pipes at the bended area (**b**) turning the pipe in 90° and zoom in to the fully damaged.

Table 2: Average tensile test results of the new and after service tube samples.

Sample	Yield stress $\sigma_{0.2}$% (MPa)	Strength R_m (MPa)	Strain ε_{fr} (%)
As-received tubes	138.5	511.3	48.1
Standard Deviation	12.58	1	1.15
After-service	87.5	376.5	35.65
Standard Deviation	5.86	12.5	0.75
Decrease in properties (%)	36.8	26.4	25.9

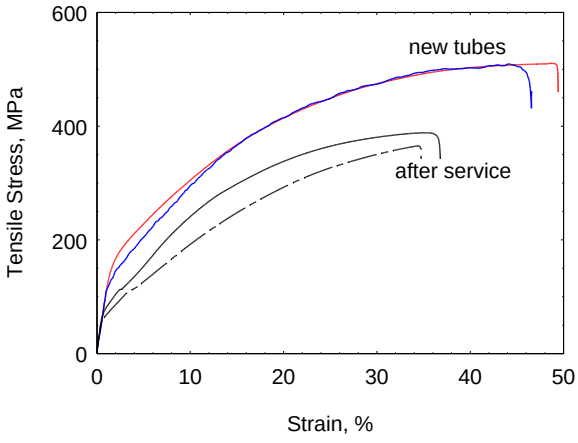

Fig. 5: Stress-strain curves of the tested new and after service Ni-200 tube.

Microstructure investigation

The optical observation of as received Ni-200 alloy (Fig. 7) shows a grained structure with relatively low twinning density. The grain size was around 35 μm. Twinning are clearly seen in some grains. This type of defect is often observed in metal and alloys with FCC structures. Twins in Ni-200 alloy under investigation are confined inside the grains, in contrarily to annealing twins that are characterized by straight

lines extending across the grain boundaries [11]. Ni-200 alloy has been reported to have a single phase and has a microstructure similar to that of austenitic stainless steel [12].

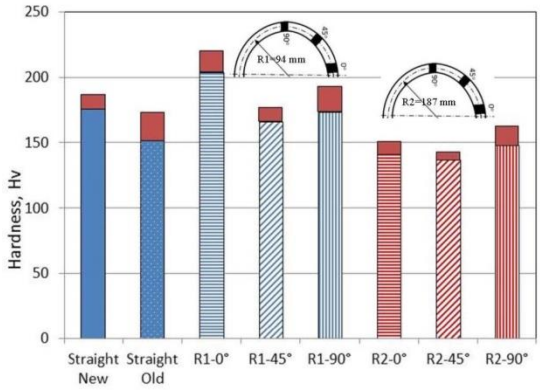

Fig. 6: Hardness distribution with error bar at different positions on the radius of curvature of the bent tubes (at 0°, 45°, 90°) as shown in Fig.3.

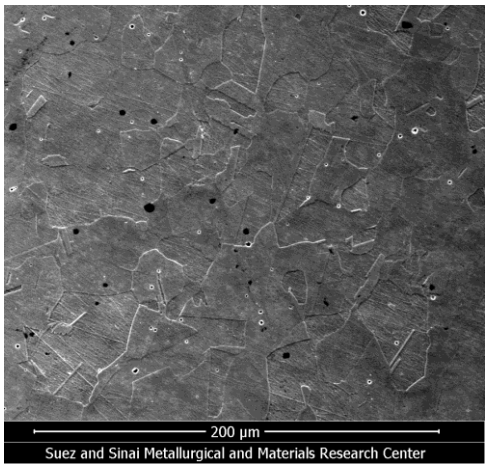

Fig. 7: Optical micrograph of the Ni 200 alloy.

Fig. 8 reveals SEM images at different sites of the damaged tube. Fig. 8a shows a region, which is slightly attacked at the outer surface, while Figs. 8b-d display severely attacked regions that led to thinning of the tube wall. At many regions, the corrosion damage caused separation of metal crusts from the outer tube.

Fig. 9 illustrates the EDX elemental analysis of corroded outer area in the tube. The EDX line analysis through the corroded area (Fig. 9c) shows that S is significantly enriched in the corrosion product, together with a noticeable presence of O. The major presence of Ni and S is ascribed due to the corrosion product of NiS, and the appearance of O in the analysis has been assigned to sulfide oxidation as a consequence of air exposure before the EDX analysis [13]. This has been evidenced by the presence of nickel sulfate as a result of exposure of NiS corrosion layer to air [13].

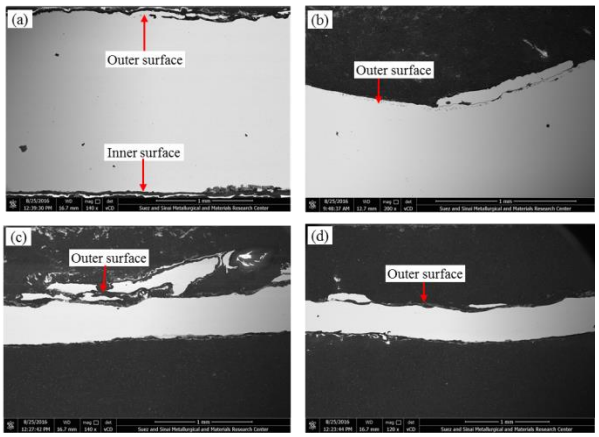

Fig. 8: SEM of polished longitudinal section through a damaged tube walls with different degree of attack.

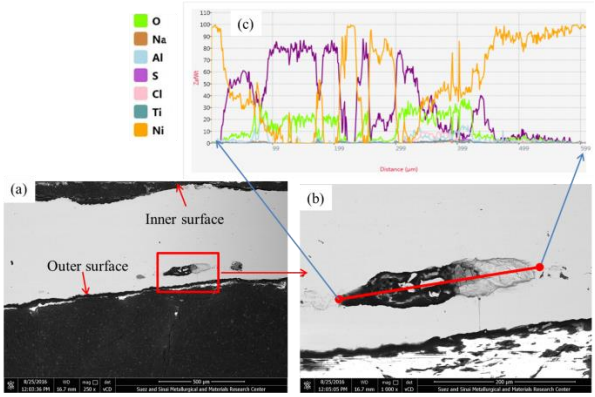

Fig. 9: (**a**) SEM of polished longitudinal section in the damaged tube wall, (**b**) higher magnification of attacked area near the tube surface, and (**c**) EDX line scan through the attacked region.

NiS has been found to be formed when Ni and Ni alloys are exposed to sulfur species-contained solutions. NiS is a porous film and has no passivation characters. It is reported that the adsorbed S species catalysis the dissolution of Ni and inhibits its passivation [13,14]. S species can be found as HS^- or H_2S in acidic solutions and as metastable $S_2O_3^{2-}$ or stable SO_4^{2-} anions in neutral and alkaline solutions [15]. Moreover, S and Cl species, in chloride-contained solutions, can interact with the passive film/solution interface; they have a combined effect on film degradation [15,16].

Failure precursors and operating conditions

Referring to the operating conditions, the $TiCl_4$ fluid reaches its highest temperature in the left side of vaporizer (Fig. 1) where it flowed for the longest path in contact with the heating tubes. Furthermore, $TiCl_4$ is exposed to a relatively higher heating surface density at U-bend tubes in the left side of the vaporizer. Thus, $TiCl_4$ temperature is expected to increase in this region to temperatures equal to or higher than the boiling point of $TiCl_4$. In addition to this increase in temperature, the decrease in the hydrostatic pressure to "P_2" due to lowering of liquid $TiCl_4$ level to "h_2" (Fig. 1) can be less than the vapor

pressure of $TiCl_4$. As a result, vapor bubbles are created and begin to rise up, yet the vapor bubbles collapse when they touch the side part of upper tubes resulting in cavitation corrosion, as seen in Fig. 2a. Vapor bubbles may also collapse by subsequent pressure increase.

Cavitation corrosion causes breakdown of the passive film and rather results in attack on the base metal that leads to thinning of the tube reaching to its crack. The corrosion by sulfur is speculated to occur simultaneously as a lateral mechanism on the bottom of the cavities that act as anodic area free from the passive film. Furthermore, thinning of the tubes can lead to steam leakage that may result in hydrolysis of $TiCl_4$ according to the equation [17]:

$$TiCl_4 + 2\ H_2O \rightarrow TiO_2 + 4\ HCl$$

Eventually, leakage of H_2O results in an aqueous acidic medium, and furthermore it can react with S species forming H_2S that reacts with Ni as stated in the reaction [13]:

$$Ni + H_2S \rightarrow NiS + H_2,$$

and this can interpret formation of nickel sulfide as a corrosion product.

Conclusions

Failure of Ni-200 tubes occurred in titanium tetrachloride vaporizer after 6 months in service.

Optical investigation showed that the tubes encountered cavitation corrosion in the upper part of U-bent tubes. Variation of hydrostatic pressure associated with operation conditions led to formation and collapse of gaseous $TiCl_4$ bubbles on the Ni-200 tube surface.

Hardness and tensile tests demonstrated that the used tubes had lower mechanical properties compared to the new tubes. Additionally, the bent tubes manifested strain hardening conditions that can make it a potential site for corrosion.

SEM/EDX investigations of the damaged sections showed that sulfur was significantly enriched in the corrosion product layer that is mainly composed of NiS.

It can be stated that the cavitation corrosion is the main and initiative attack mechanism that led to active cavities on Ni surface, which reacted with sulfur species present in liquid titanium chloride forming NiS.

It is recommended to keep the fluid at a high pressure so that the vapor bubbles are not formed. Also, the sulfur content in the $TiCl_4$ must be kept at lower levels.

References

[1] H. Alves, U. Heubner, Aqueous corrosion of nickel and its alloys, Reference module in materials science and materials engineering (2016) 1879-1915.

[2] G. Gece, S. Bilgic, A theoretical study on the inhibition efficiencies of some amino acids as corrosion inhibitors of nickel, Corrosion Science 52 (2010) 3435–3443.

[3] O.O. Igea, S. Aribo, B.A. Obadele, T. Langa, P.A. Olubambi, Erosion-corrosion characteristics of spark plasma sintered pure nickel in simulated mine water, Tribology International 109 (2017) 441–446.

[4] S.R. Addanki, A.K. Lahiri, T. Banerjee, Corrosion of nickel in steam condensate containing air and Carbon dioxide. NML Technical Journal, 3 (4) (1961) 21-24.

[5] I.I. Ivanov, O.A. Dubovikov, L.V. Grigoreva, A.A. Kuzhaeva, P.V. Zgonnik, Study of stability of constructional materials in melts containing lower titanium chlorides, Russian J. Applied Chemistry 84, 9 (2011) 1529−1531.

[6] A.A. Kuzhaeva, L.V. Grigorieva, The effect of titanium chlorides on corrosion resistance of materials, Int. J. Applied Eng. Res. 11, 9 (2016) 6210-6213.

[7] S.N.F. Mazlan, A. Ismail, L.M.N. Lokman, S. Ahmad, Failure Analysis on Heat Exchanger Tube Bundle Exposed to Naphthenic Acid Corrosion, Key Eng. Materials 791 (2018) 95-101.

[8] X.-L. Yang, Y. Gong, Q. Tong, Z.-G. Yan, Failure analysis on abnormal bursting of heat transfer tubes in spiral-wound heat exchanger for nuclear power plant, Eng. Failure Analysis, in press https://doi.org/10.1016/j.engfailanal.2019.104298

[9] M. Schwartz , Four types of heat exchanger failures, Plant Engineering Magazine, December 23, 1982 (https://www.deppmann.com/home/wp-content/uploads/2016/10/4-Types-of-Heat-Exchanger-Failures-article.pdf)

[10] D.S. Janikowski, Selecting Reliable Heat Exchanger Tube Materials – Factors to Consider, API Power Chem 2014 Novotel Twin Waters, Sunshine Coast, Queensland, May 27, 2014. (https://www.plymouth.com/wp-content/uploads/2017/03/Reliable-Exchanger-Tubing-Powerchem-2014-Janikowski-1.pdf)

[11] A. Gunen, E. Kanca, Microstructure and mechanical properties of borided Inconel 625 superalloy, Matéria (Rio de Janeiro) 22, 2 (2017) 22 (2). http://dx.doi.org/10.1590/s1517-707620170002.0161

[12] F.G. Hodge, The history of solid-solution-strengthened Ni alloys for aqueous corrosion service, JOM: The Journal of The Minerals, Metals & Materials Society (TMS) 58 (2006) 28-31.

[13] M. Monnot, R.P. Nogueira, V. Roche, G. Berthome, E. Chauveau, R. Estevez, M. Mantel, Sulfide stress corrosion study of a super martensitic stainless steel in H2S sour environments: Metallic sulfides formation and hydrogen embrittlement, App. Surf. Sci. 394 (2017) 132–141.

[14] X. Cheng, H. Ma, S. Chen, X. Chen, Z. Yao, Corrosion of nickel in acid solutions with hydrogen sulphide, Corrosion Sci. 42 (2000) 299-311

[15] D.-H. Xia, Y. Behnamian, J.-L. Luo, Review—Factors influencing sulfur induced corrosion on the secondary side in pressurized water reactors (PWRs), J. Electrochem. Soc. 166, 2 (2019) C49-C64.

[16] Y.-B. Zhang, X.-L. Yang, A. Tang, Corrosion behavior of nickel-based 718 alloy determined by in situ electrochemical methods at different partial pressures of H2S in 25 wt% NaCl solution at 150oC, Rare Met. (2019) 38, 9 (855–863).

[17] J. Yuan, M. Chen, J. Shi, W. Shangguan, Preparations and photocatalytic hydrogen evolution of N-doped TiO2 from urea and titanium tetrachloride, Int. J. Hydrogen Energy 31, 10 (2006) 1326-1331.